PROCEEDINGS OF THE ROYAL SOCIETY A

Proc. R. Soc. A (2007) **463**, 641–658
doi:10.1098/rspa.2006.1781
Published online 31 October 2006

Rubber band recoil

By R. Vermorel, N. Vandenberghe* and E. Villermaux†

IRPHE, Aix-Marseille Université, CNRS, 49 rue Joliot-Curie, F-13384 Marseille Cedex, France

When an initially stretched rubber band is suddenly released at one end, an axial-stress front propagating at the celerity of sound separates a free and a stretched domain of the elastic material. As soon as it reaches the clamped end, the front rebounds and a compression front propagates backward. When the length of the compressed area exceeds Euler critical length, a dynamic buckling instability develops. The rebound is analysed using Saint-Venant's theory of impacts and we use a dynamical extension of the Euler–Bernoulli beam equation to obtain a relation between the buckled wavelength, the initial stretching and the rubber band thickness. The influence of an external fluid medium is also considered: owing to added mass and viscosity, the instability growth rate decreases. With a high viscosity, the axial-stress front spreads owing to viscous frictional forces during the release phase. As a result, the selected wavelength increases significantly.

Keywords: rubber band; elastic instability; dynamic buckling

1. Introduction

In his classical treatment of the *elastica*, Euler (1744) proved that for a given length and for given boundary conditions, there exists a critical load at which a rod buckles. Among the different possible bent shapes, only the one with the smallest number of inflections is stable, i.e. the shape corresponding to the fundamental flexural mode (e.g. Love 1944). Thus, the only characteristic length associated with the buckling instability is the length of the rod itself.

However, when a compressive load several times higher than the Euler critical force is suddenly applied to an *elastica* at rest, the buckling instability develops dynamically and a characteristic wavelength is selected. Lindberg (1965) studied the growth of the different flexural modes of an Euler–Bernoulli beam suddenly compressed. The theory predicts that the most amplified wavelength decreases like the inverse square root of the compression strain. He also devised an ingenious way to determine the buckled wavelength from experiments on metallic elastic beam and on rubber bands. In the case of the metallic beam, he found a fair agreement with theory, while in the case of the rubber band, discrepancies were stronger: the measured wavelength was 70% higher than predicted for reasons that were not elucidated.

* Author for correspondence (nvdb@irphe.univ-mrs.fr).
† Also at Institut Universitaire de France.

Electronic supplementary material is available at http://dx.doi.org/10.1098/rspa.2006.1781 or via http://www.journals.royalsoc.ac.uk.

Received 19 July 2006
Accepted 21 September 2006

The aim of the present work is to study in detail the dynamic buckling instability responsible for the recoil of a rubber band. Indeed, the rubber band is an interesting system for the study of dynamic buckling because the characteristic speed of sound in rubber is moderate (about 40 m s^{-1}) and strains and displacements can be large. It also represents a simple case study of more general situations where flexural and compression waves are coupled, as those encountered in the related problem of brittle rod fragmentation under impact (Gladden *et al.* 2005). The question is envisaged in its most general setting, including the influence of a surrounding medium as we perform experiments in air and in liquids, namely water and water–glycerol mixtures to investigate the effect of added mass and fluid viscosity.

2. Experimental set-up

We first consider the recoil of a cantilever rubber band. One end of the rubber band is firmly clamped on the experimentation table. The operator holds the free end, stretches the elastic to the desired length and releases it suddenly. A set-up was also designed to stretch and release the rubber band from both ends simultaneously. A thin fishing line is glued to both ends of the elastic in such a way that the line and the elastic material form a loop. This loop is placed around two pulleys. Thus, the operator can stretch and release the rubber band by pulling and dropping the fishing line.

The elastics were cut from natural latex rubber sheets of thicknesses from 0.254 up to 1.270 mm. The length and width of the rubber bands are $\ell_0 = 150$ mm and $b = 4$ mm. The measurement of the force-extension curve reveals that in the range of stretching between 0 and 100%, the elastic behaviour of the rubber remains linear (within 3%) with the Young modulus $E = 1.5$ MPa and no significant hysteretic behaviour or stress softening of the rubber (Bouasse & Carrière 1903; also called the Mullins effect after Mullins 1947) were observed. For higher stretching, significant deviation from the ideal Hookean behaviour was observed and in most experiments, the stretching has been limited to the range 0–100%. The density of the rubber is $\rho = 990$ kg m^{-3} and thus the nominal wave speed for longitudinal disturbances is $c = (E/\rho)^{1/2} = 39$ m s^{-1}.

We used a Phantom V5 high-speed video camera to record movies at typical frame rates of 10 000–30 000 frames per second. The rubber band is illuminated from behind using a white light source and a diffusing screen or by direct lighting using a black or white background. Regularly spaced marks are drawn on the elastic to follow the motion of the material points.

To study the influence of the external medium, experiments were also conducted with the set-up immersed in a tank filled with water or with water–glycerol mixtures of controlled viscosity. Viscosities were measured using a Couette viscosimeter and we used viscosities from $\eta = 1.0 \times 10^{-3}$ (pure water) up to 6.5×10^{-1} Pa s.

3. Recoil of a rubber band in air

(a) *Phenomenology*

Stretching and releasing a rubber band is a common experience. The typical time-scale of this phenomenon is $\ell_0/c \approx 3.8$ ms, hence the use of high-speed imaging. When the tension is suddenly released, a front propagates towards the clamped end

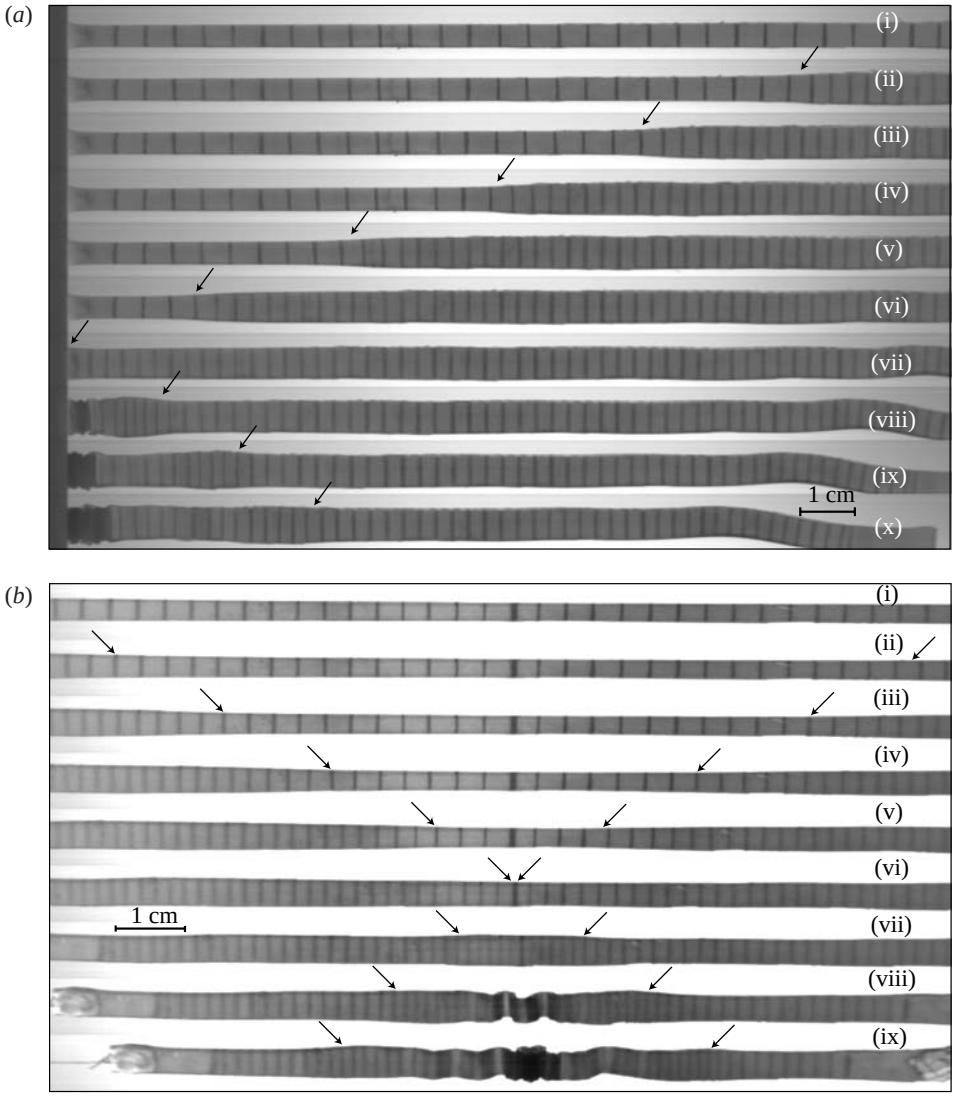

Figure 1. (*a*) Front propagation in a clamped rubber band with initial stretch $\epsilon_0=1$. (i)–(vi) The front (marked by the arrow) propagates towards the clamped end and drags the free region. (vii) When the front reaches the clamped end, the strain-free rubber band moves towards the clamped end. (viii)–(x) After impact, a compressive front propagates backward and triggers a dynamic buckling instability. Time proceeds in steps of 350 μs. A movie showing the front propagation is included in the electronic supplementary materials. (*b*) Fronts propagation in a rubber band simultaneously released from both ends with $\epsilon_0=1$. The two fronts (marked by the arrows) propagate towards the middle of the elastic. (vi) When the fronts cross each other, compressive fronts set out from the middle (vii)–(ix) and trigger buckling. Time proceeds in steps of 320 μs.

(figure 1*a*, images (i)–(vi)) at the celerity c in the material. The front separates two regions: a stress-free area between the free end and the front, and a stretched area between the front and the clamped end. As the front propagates, it drags the free region down to the clamped end at velocity V, which is a fraction of c.

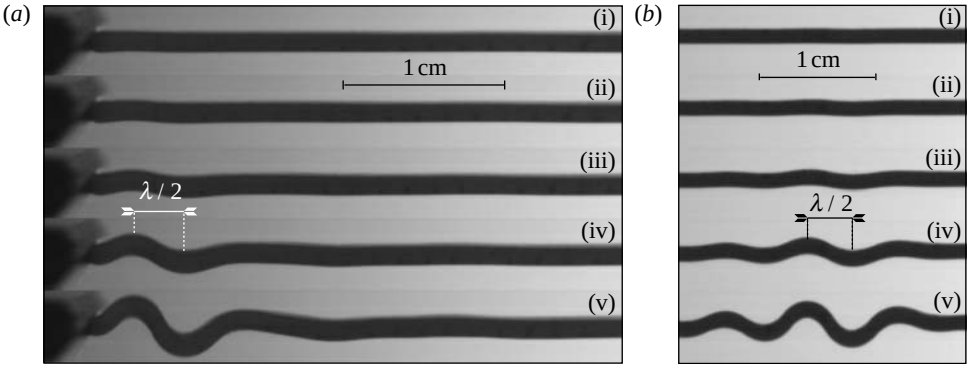

Figure 2. (*a*) Early stages of the dynamic buckling of a clamped rubber band with $\epsilon_0 = 0.3$. Time proceeds in steps of 117 μs. (*b*) Early stages of the dynamic buckling of a rubber band simultaneously released from both ends with $\epsilon_0 = 0.2$. Time proceeds in steps of 130 μs. A movie showing the dynamic buckling is included in the electronic supplementary material.

When the front reaches the clamped end, the whole rubber band is free, moving towards the table at velocity V (figure 1*a* (vii)). The configuration is then equivalent to a free rubber band moving at velocity V impacting a rigid surface (see Saint-Venant & Flamant (1883) and references therein). A compressive front propagates towards the free end at speed c in the frame of the rubber band (figure 1*a* (viii)–(x)). Between the clamped end and the front, the elastic is compressed. As soon as the compressive front has travelled a critical distance from the clamped end, the compressive stress is applied to a region long enough to trigger off a buckling instability. The elastic starts to bend with a well-defined wavelength (figure 2 (iv)). The first complete half wavelength will be referred to as the half-buckled wavelength. Thereafter, the front propagates towards the free end inducing more bending of the rubber band. Our focus is on the first half wavelength only because the subsequent dynamics becomes more complicated. In particular, near the clamped end, the transverse displacement resulting from the buckling is coupled to the propagation of the longitudinal wave.

To check the influence of the boundary conditions on the dynamics, we performed a similar experiment with a rubber band simultaneously released from both ends. Two fronts propagate towards the middle of the elastic. When the fronts reach the middle, the rubber band is stress-free but its two halves are moving with opposite velocities V and $-V$. The configuration is then equivalent to the classical problem of two rods impacting each other. Compressive fronts propagate away from the junction (i.e. the middle of the rubber band), triggering the dynamic buckling instability in both sides of the rubber band. Our measurements show that the dynamics is strictly identical to the case of the clamped rubber band for low stretching (less than 50%). For higher stretching, the friction of the fishing line sliding against the axes results in a slight decrease of the velocity of the free regions of the rubber band. Therefore, all the measurements reported in this paper were obtained with the more reliable clamped-free configuration.

(*b*) *Compression front*

The rubber band is modelled as a Hookean elastic rod experiencing small strain. We neglect the effect of lateral inertia and we use the small strain

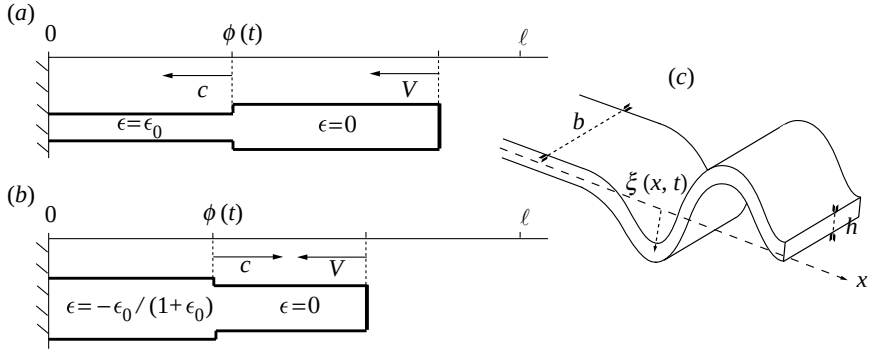

Figure 3. (*a*) Schematic of the stress-free front propagation. ℓ is the length of the stretched rubber band. ϕ is the position of the front. The stress-free front propagates towards the clamped end at speed of sound c and it drags the free region with a constant velocity V. (*b*) The rebounding front propagating backward. (*c*) Schematics of the dynamic buckling of a rubber band. b and h are the width and the thickness of the band, respectively. ξ is the transverse displacement.

hypothesis. Thus, longitudinal perturbations are governed by the linear wave equation with the propagation speed c. A more refined model for the front propagation can be used, but for the range of stretching $\epsilon_0 \leq 1$, the simplest model offers an accurate description of the dynamics (e.g. Mason 1963).

Let ℓ be the length of the stretched rubber band and ℓ_0 its length at rest. The initial strain ϵ_0 is

$$\epsilon_0 = \frac{\ell - \ell_0}{\ell_0}. \tag{3.1}$$

The front is a discontinuity that separates a strain-free region and a stretched region in which $\epsilon = \epsilon_0$ (figure 3*a*). The front propagates at speed c and it reaches the anchor point at time $t_i = \ell/c$. Then the elastic is strain-free and its length is ℓ_0. V being the speed of the free end, we have $\ell - \ell_0 = -Vt_i$ and thus we obtain that

$$V = -\left(\frac{\ell - \ell_0}{\ell}\right) c = -\left(\frac{\epsilon_0}{1+\epsilon_0}\right) c. \tag{3.2}$$

This relation holds for all material points in the free region.

When the front reaches the clamped end, the whole rubber band is strain-free and translates at speed V. Thus, the problem is equivalent to a rubber band impacting a rigid surface at speed V. Let $\zeta(x, t)$ be the longitudinal displacement in the rubber band. x is the coordinate of a material point along the rod with $x=0$ being the anchor point. When the front reaches the $x=0$ position, all the points of the elastic are moving at speed V. At time $t=0$, the front suddenly encounters a $\zeta(0, t)=0$ condition. It rebounds and propagates backward at speed c (in the material frame, i.e. it is propagating at speed $c+V$ in the laboratory frame with $V<0$). The front propagating away from the 'impact point' separates a compressed area in which the speed is zero and a stress-free area moving at speed V (figure 3*b*). At time t, the front has reached the point $x=\phi=ct$ and this point has been displaced by a quantity $\zeta(x, t) = Vt = Vx/c$. Thus, the strain in the compressed area is

$$\epsilon = V/c = -\epsilon_0/(1+\epsilon_0). \tag{3.3}$$

Behind the rebounding front, the compressive force is given by Hooke's law

$$T = \sigma bh = -Ebh\epsilon_0/(1+\epsilon_0), \tag{3.4}$$

where b and h are the width and thickness of the rubber band.

(c) Mode selection

We introduce an equation for the transverse displacement $\xi(x, t)$ (figure 3*c*) by plugging the above compressive force into the equation describing the dynamics of the bending waves and using Euler–Bernoulli description

$$\rho bh\frac{\partial^2\xi}{\partial t^2}-\frac{\partial}{\partial x}\left(T\frac{\partial\xi}{\partial x}\right)+EI\frac{\partial^4\xi}{\partial x^4}=0, \tag{3.5}$$

where $I=bh^3/12$ is the flexural inertia momentum in the flexion plane.

We look for solutions of the form $\xi(x, t)=\xi_0\exp(\mathrm{i}kx-\mathrm{i}\omega t)$. With T constant along the rod, the dispersion relation reads

$$\omega^2=\frac{EI}{\rho bh}k^2\left\{k^2+\frac{T}{EI}\right\}. \tag{3.6}$$

For a compressive force, T is negative. Unstable modes have wavenumbers in the range 0 to k_c where k_c is the marginal wavenumber,

$$k_\mathrm{c}=\sqrt{\frac{|T|}{EI}}. \tag{3.7}$$

The most amplified wavenumber is $k_\mathrm{m}=k_\mathrm{c}/\sqrt{2}$, so that, making use of equation (3.4) for T, the most amplified wavelength writes, mutatis mutandis

$$\lambda_\mathrm{m}=\pi h\sqrt{\frac{2}{3}}\sqrt{\frac{1+\epsilon_0}{\epsilon_0}}, \tag{3.8}$$

and its associated growth rate is

$$\sigma_\mathrm{m}=\sqrt{3}\frac{\epsilon_0}{1+\epsilon_0}\frac{c}{h}. \tag{3.9}$$

The selected mode depends on both the material elastic properties and intensity of the compression, but since the compression is itself a function of the material elasticity, a cancellation effect makes λ_m depend on geometrical parameters only, namely the thickness of the rubber band and initial stretching.

Of course, this naive expectation assumes that the compression front has travelled by a distance at least equal to λ_m during a time lapse given by σ_m^{-1}. A more general mode-selection criterion would thus be that the amplified wavenumber k is the one for which

$$\tau(k)c\simeq k^{-1}, \tag{3.10}$$

and $k=k_\mathrm{m}$ otherwise if $\tau(k)c\gg k^{-1}$. There, $\tau(k)$ is the instability time-scale associated with k through the dispersion relation (3.6) such that $\tau(k)^{-1}=\mathrm{Re}\{-\mathrm{i}\omega\}$.

The above reasonings are made within the long wave approximation ($kh\ll1$) and disregard three-dimensional effects when the wavelength becomes of the order of the thickness h, as it is nevertheless the case for the higher initial elongations ϵ_0. We also do not account for any coupling between the instability development and the compression force, nor any nonlinear elastic response of the material. Finally, the model based on a constant compression force T gives satisfactory results and it was not necessary to couple explicitly the axial front propagation with the buckling dynamics (as in Lepik (2001) and Vaughn & Hutchinson (2006)).

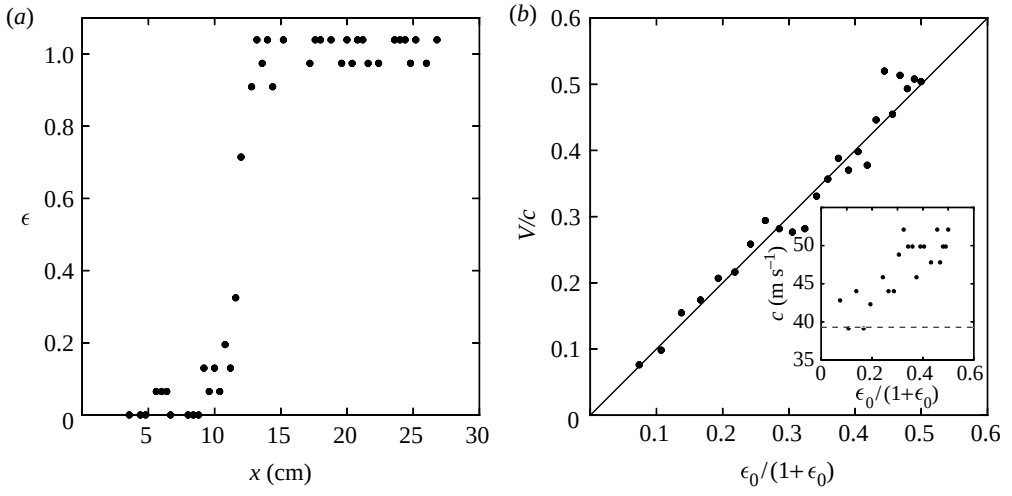

Figure 4. (*a*) Stretch profile during the propagation of the stress-free front. x is the material coordinate. (*b*) Ratio V/c versus $\epsilon_0/(1+\epsilon_0)$. The dots stand for the measurements and the line stands for the theoretical prediction with no adjusted parameters. Here, c is the measured front speed which is slightly higher than $(E/\rho)^{1/2} \approx 39\ \mathrm{m\,s^{-1}}$ (see insert).

(*d*) *Experimental results*

To measure the propagation speeds, we draw regularly spaced marks along the rubber band (figure 1). The theoretical value of the front velocity for the rubber bands that we used in the experiments is $39\ \mathrm{m\,s^{-1}}$, which is in agreement with the measurements for small initial stretching. However, the speed of the front is slightly higher, typically $50\ \mathrm{m\,s^{-1}}$, in particular, for high initial stretching ($\epsilon_0 \geq 0.6$). This is probably due to the effect of the strain rate on the elongational modulus known in rubber (Kolsky 1949), not taken into account here.

The measured value of V typically ranges from 4 to $20\ \mathrm{m\,s^{-1}}$, depending on the initial stretch (figure 4*b*). The evolution of the ratio V/c (c is the measured front speed) is in fair agreement with the theoretical prediction. Measurements of the stretching profile show that the front shape is well approximated by a step function (figure 4*a*). Actually, the dependency of V on initial stretch ϵ_0 found in §3*b* is valid even for high initial stretching ($\epsilon_0 \simeq 1$), i.e. beyond the limitations of the small strain hypothesis.

The first selected wavelength was obtained for rubber bands of thickness from 0.254 up to 1.27 mm, for an initial stretch $\epsilon_0 = 0.2$ (figure 5*a*). All properties and dimensions of the rubber bands are the same but their thickness. We find that $\lambda_\mathrm{m} \sim h$ as expected. Figure 5*b* shows the experimental wavelengths obtained with a rubber band of thickness $h = 1.27$ mm. Experimental results agree with the prediction from equation (3.8) for small initial stretching (i.e. for high $(1+\epsilon_0)/\epsilon_0$ ratio). However, for large initial stretch (i.e. for $(1+\epsilon_0)/\epsilon_0$ smaller than 4), the measured wavelengths are shorter than predicted from equation (3.8). A better fit is obtained considering a mode-selection criterion based on the length travelled by the re-compression front given in equation (3.10). For even higher initial stretch (i.e. for $(1+\epsilon_0)/\epsilon_0 < 2$), the wavelength becomes of the order of the band thickness and the long wave approximation breaks down.

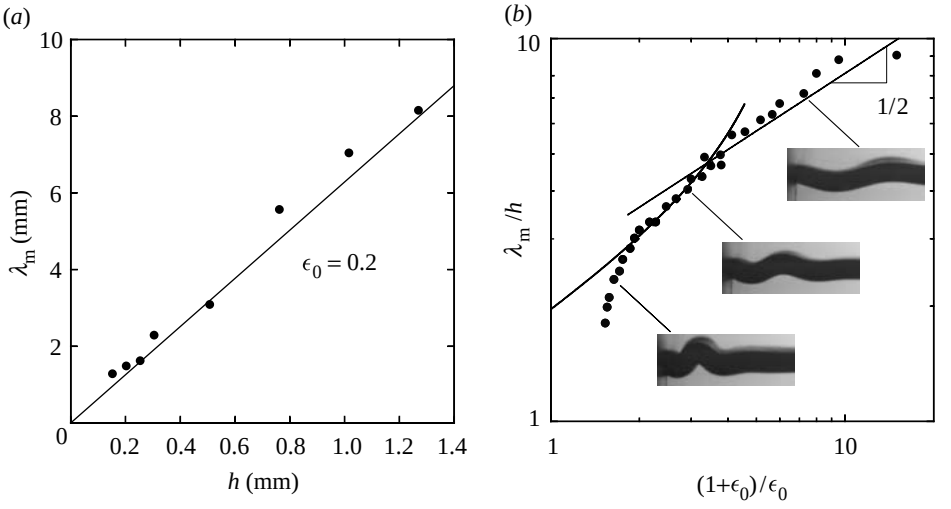

Figure 5. (*a*) Variation of the selected wavelength λ_m with the thickness of the rubber band h. The straight line stands for the theoretical curve with no adjusted parameters. (*b*) Variation of the selected wavelength λ_m with the initial stretch ϵ_0. The straight line stands for the theoretical curve from equation (3.8) with no adjusted factor. The curve fit is from equation (3.10) with $\tau(k)c = 2.6\ k^{-1}$.

Note that using a dispersion relation that includes both Rayleigh's correction (rotational inertia) and Timoshenko's correction (effect of shear stress) leads to even higher wavelengths (e.g. Graff 1975). Finally, once the band is wrinkled, the axial stress relaxes by a simple geometrical effect, as suggested by figure 1 (viii) and (ix)). This leads to a coarsening of the initial wrinkled pattern, a phenomenon which is probably at the origin of Lindberg's strong discrepancy between the anticipated and measured wavelength.

4. Recoil of a rubber band in fluids

Several new effects are expected in the presence of an external fluid. First, when the instability develops, fluid must be moved together with the rod and thus we expect added mass effects. Moreover, if the fluid is viscous, we expect damping. In this section, we modify the analysis of §3 to account for these ingredients. As we shall see, in order to accurately describe the dynamic of the rubber band in a fluid, we must also consider the effect of viscosity on the axial-stress front propagation.

(*a*) *Modification of the instability*

We consider a thin rod under compressive stress surrounded by an external fluid. We use the same hypotheses and notations as in §3*b*. The fluid is Newtonian and incompressible, of density ρ_f and of kinematic viscosity ν. The dispersion equation in non-dimensional form (appendix A) reads

$$(k_* + 4M)\sigma_*^2 + 4\chi k_* \left[k_* + \left(\frac{M}{\chi}\sigma_* + k_*^2 \right)^{1/2} \right] \sigma_* + 4k_*^3 \left(k_*^2 - 1 \right) = 0, \qquad (4.1)$$

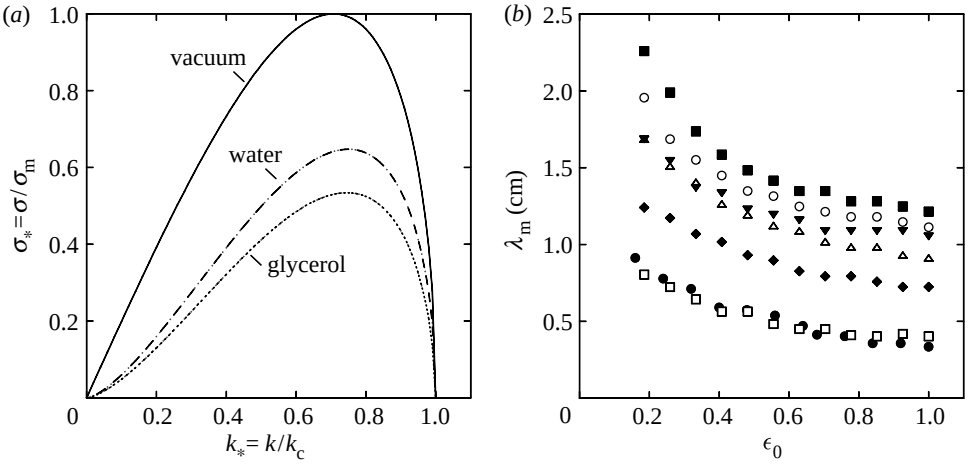

Figure 6. (*a*) Predicted non-dimensional growth rate σ_* versus non-dimensional wavenumber k_*. For vacuum, $\chi=0$ and $M=0$; for water, $\chi=3.5\times10^{-5}$ and $M=0.25$; and for glycerol, $\chi=2\times10^{-2}$ and $M=0.35$. (*b*) Measurements of the selected wavelength λ_m versus initial stretch ϵ_0 for different fluids: filled circle, air; open square, water; filled diamond, glycerol $\eta=0.04$ Pa s; open up triangle, glycerol $\eta=0.190$ Pa s; filled down triangle, glycerol $\eta=0.650$ Pa s; open circle, glycerol $\eta=0.450$ Pa s; filled square, glycerol $\eta=0.650$ Pa s.

where $k_*=k/k_c$ and $\sigma_*=\sigma/\sigma_m$. M and χ are two non-dimensional numbers related to the added mass term and the viscous term, defined as

$$M=\frac{\rho_f}{4\pi\rho k_c h},\quad \chi=\left[\frac{\eta^2 b}{\rho|T|h}\right]^{1/2}, \tag{4.2}$$

where $T=-Ebh\epsilon$. χ depends on the dynamic viscosity $\eta=\rho_f\nu$ of the fluid and on the Young modulus E, density ρ, thickness h and extensional strain of the rod (but b cancels out in the expression for χ, when T is expressed in terms of E).

Figure 6 shows the dispersion relation obtained in different fluids (note that the glycerol we used was not pure and its dynamic viscosity was $\eta=0.65$ Pa s). The viscous number χ is rather small ($\chi=0.02$ for a dynamic viscosity $\eta=0.65$ Pa s). Therefore, the main effect of the external fluid is the added mass effect that results in a significant decrease of the instability growth rate. Compared with the theoretical value in vacuum, growth rate should decrease by a factor 1.6 for water and almost a factor 2 for glycerol. On the other hand, the selected wavelength is not significantly modified by the interaction with the external fluid. For high χ numbers (i.e. for high viscosity), the selected wavenumber decrease to an asymptotic value, $k_{*\,m}\sim1/\sqrt{3}$ instead of $k_{*m}=1/\sqrt{2}$ with no external medium. The added mass tends to increase the selected wavenumber and for high values of M, k_{*m} goes to $\sqrt{3/5}$.

(*b*) *Experiments in fluids*

We conducted experiments in water, and in water–glycerol mixtures with viscosity ranging from $\eta=4\times10^{-2}$ up to 0.65 Pa s. Figure 6*b* shows wavelengths measured in air, water and water–glycerol mixtures. In water, the results are

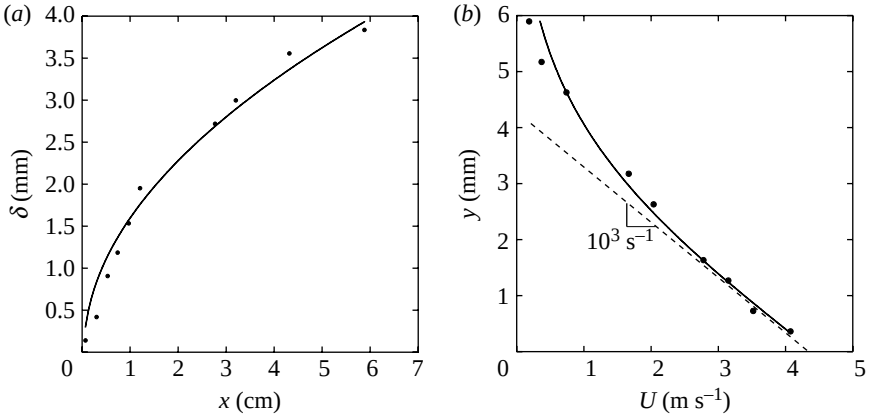

Figure 7. (*a*) Thickness of the boundary layer δ versus axial coordinate x at one instant of time. The origin for x is the position of the stress-free front. The continuous line is a square root fit. (*b*) Velocity profile in the boundary layer at the position $x=85$ mm and 13 ms after the passage of the front. Data is fitted by a function of the form $U_0(1-\mathrm{erf}(y/\delta))$ and we find $\delta=4.74$ mm, which is close to the theoretical prediction $(4\nu[t-x/c])^{1/2}=4.89$ mm.

similar to those performed in air. With more viscous fluids, we observe a significant increase of the selected wavelength. The wavelength is more than doubled in the glycerol ($\eta=0.65$ Pa s). As discussed above, that effect is too large to be attributed to the impact of viscosity on mode selection in the buckling instability.

To clarify the effect of viscosity on the propagation of the compression front, we visualized the flow field. Particles were added to the fluid (glycerol with dynamic viscosity $\eta=0.65$ Pa s) and the elastic was illuminated by a laser sheet. After the release of the rubber band, a boundary layer follows the axial-stress front. The spatial profile of the boundary layer in the plane of the length and thickness of the rubber band (which was the plane illuminated by the laser sheet) is shown in figure 7*a*. The profile of the boundary layer is well fitted by a square root function of the axial coordinate. A movie showing the development of the boundary layer is included in the electronic supplementary material.

Let $U(x, y, t)$ be the velocity profile in the fluid at a given instant of time and axial location. Direction y is perpendicular to the band surface located in $y=0$. Figure 7*b* shows such a profile. The viscous frictional force per unit length of the band is given by

$$\tau_{\mathrm{f}} = -2b\eta\left(\frac{\partial U}{\partial y}\right)_{y=0}, \tag{4.3}$$

the factor 2 accounting for the two sides of the band. Using the velocity gradient measured on figure 7*b* and ℓ_0 as an estimate of the length the front has gone through, an order of magnitude of the frictional force is $F_{\mathrm{f}}\sim\tau_{\mathrm{f}}\ell_0\simeq 0.5$ N. A typical value of the velocity of the free end of the rubber band is $6\ \mathrm{m\,s^{-1}}$. Thus, the order of magnitude of the drag force $F_{\mathrm{d}}\simeq b\eta U$ at the free end of the rubber band is $F_{\mathrm{d}}\simeq 1.5\times 10^{-2}$ N. Obviously, the drag force at the end is small compared with the frictional force. Moreover, the friction increases as the stress-free front propagates and as the region dragged by the front gets wider.

An equation for the longitudinal displacement ζ accounting for frictional forces is

$$\rho bh\frac{\partial^2\zeta}{\partial t^2} = Ebh\frac{\partial^2\zeta}{\partial x^2} + \tau_{\mathrm{f}}. \tag{4.4}$$

In this plane boundary layer approximation, we first neglect the contribution of the small dimension h and disregard the contribution of the corners. Let $U_0(x,\,t) = U(x,\,0,\,t) = \partial\zeta(x,\,t)/\partial t$ be the axial velocity of the band. When U_0 is a function of time, the net force per unit length applied to the band is (see Stokes (1850) cited in Lamb (1932))

$$\tau_{\mathrm{f}} = -\frac{2\eta b}{\sqrt{\pi\nu}}\int_0^\infty \frac{\partial U_0}{\partial t}(t-t')\frac{\mathrm{d}t'}{\sqrt{t'}}, \tag{4.5}$$

so that equation (4.4) becomes

$$\rho h\frac{\partial^2\zeta}{\partial t^2} = Eh\frac{\partial^2\zeta}{\partial x^2} - \frac{2\eta}{\sqrt{\pi\nu}}\int_0^\infty \frac{\partial^2\zeta}{\partial t^2}(t-x/c-t')\frac{\mathrm{d}t'}{\sqrt{t'}}, \tag{4.6}$$

where t has been replaced by $t-x/c$ (where c is the velocity of the front) because the viscous term vanishes for $t<x/c$, i.e. when the front has not yet reached the material point x.

Now, this integro-differential equation can be simplified by considering figure 7 suggesting that the transverse velocity profile in the fluid is, in fact, very close to that developing over a plate initially at rest and moved suddenly at $t=x/c$ at a constant velocity (Stokes 1850),

$$U(x,\,y,\,t) \approx U_0(x,\,t)\left\{1-\mathrm{erf}\left(\frac{y}{\sqrt{4\nu(t-x/c)}}\right)\right\}. \tag{4.7}$$

Then, using equation (4.7), we obtain in place of equation (4.4)

$$\rho h\frac{\partial^2\zeta}{\partial t^2} = Eh\frac{\partial^2\zeta}{\partial x^2} - \frac{2\eta}{\sqrt{\pi\nu(t-x/c)}}\frac{\partial\zeta}{\partial t}. \tag{4.8}$$

This equation has no analytic solution. However, if we focus on the long time dynamics for $t\gg x/c$ (far from the front and close to the released end) and therefore neglect inertia, an asymptotic solution can be found. Equation (4.8) being linear, the stretch $\epsilon=\partial\zeta/\partial x$ obeys the same equation as the longitudinal displacement ζ, thus, in the above mentioned limit

$$\frac{\partial\epsilon}{\partial T} = D\frac{\partial^2\epsilon}{\partial x^2}, \tag{4.9}$$

where $D=Eh\sqrt{\pi\nu}/(3\eta)$. We use the time-scale $T=t^{3/2}$ and consider that $\epsilon(0,\,t)=0$. Then the asymptotic solution is

$$\frac{\epsilon(x,\,T)}{\epsilon_0} = \mathrm{erf}\left\{\frac{x}{2\sqrt{DT}}\right\}, \tag{4.10}$$

which implies that the width of the front scales like $T^{1/2}=t^{3/4}$ for large propagation time. Integrating $\epsilon(x,\,T)$ with respect to x, we find the expression for the displacement ζ,

$$\zeta(x,\,T) = \epsilon_0 x\,\mathrm{erf}\left\{\frac{x}{2\sqrt{DT}}\right\} + \frac{2\epsilon_0\sqrt{DT}}{\sqrt{\pi}}\exp\left\{-\frac{x^2}{4DT}\right\}, \tag{4.11}$$

which implies that the displacement of the free end of the rubber band goes like $T^{1/2}=t^{3/4}$ for large propagation time. The consistency of the inertialess

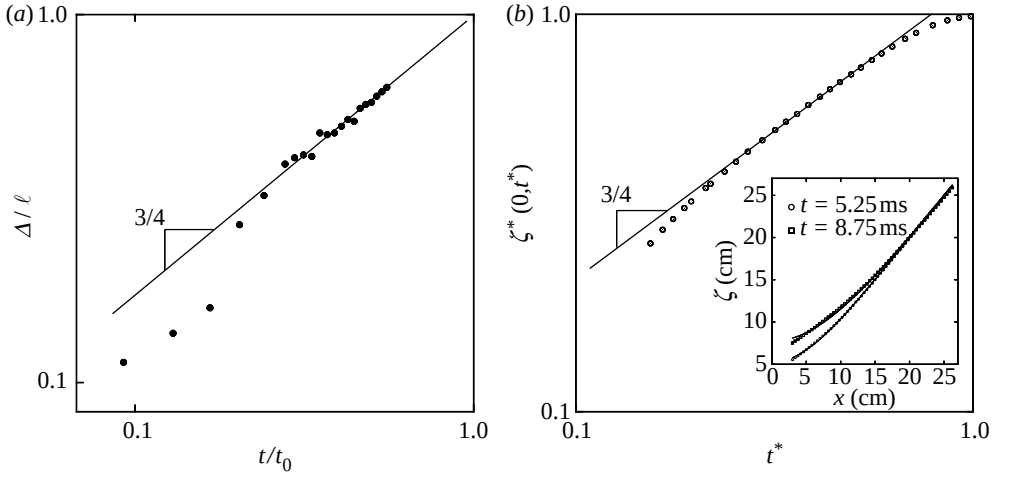

Figure 8. (*a*) Dimensionless width Δ/ℓ versus dimensionless time t/t_0. ℓ is the length of the stretched rubber band and t_0 is the time such that $Dt_0^{3/4} = \ell^2$. Δ is obtained by fitting the strain front profile (see text). (*b*) Dimensionless displacement at the free end versus dimensionless time. The front profile is well fitted by expression (4.11) (insert) and displacement of the free end goes like $t^{3/4}$ at large times.

approximation is justified *a posteriori* noticing that both the terms retained in the balance of equation (4.9) are of order ϵT^{-1} while the inertial term is of order $\epsilon T^{-4/3}$, i.e. subdominant at large time.

The displacement and the strain were measured by tracking the motion of marks drawn on the rubber band. For different values of time, the strain profile is fitted by a function $\mathrm{erf}(x/\Delta)$ and the values of Δ are plotted on figure 8*a*. For sufficiently large time, we observe the expected behaviour $\Delta \sim t^{3/4}$. The displacement front is well fitted by expression (4.11) and that of the free end proceeds like $t^{3/4}$ at large times.

However, in all cases, the apparent coefficient in front of $\sqrt{Dt}$ was about half the expected one. This deviation indicates that the experimental friction is larger than the one anticipated by approximating the total friction as the sum of the two boundary layers friction on both sides of the band (equations (4.3) and (4.4)). The reason is the influence of the band section corners, negligible at short time, but contributing by an amount of the same order than the one from the boundary layers when their thickness δ becomes comparable to the width b. The total friction per unit length writes in fact (in the limit $h \ll b$)

$$\tau_{\mathrm{f}} = 2\eta \frac{U_0 b}{\sqrt{\pi \nu t}} \left(1 + \frac{2\sqrt{\nu t}}{\sqrt{\pi} b}\right), \tag{4.12}$$

and is indeed twice that obtained by simply adding the plane boundary layers contributions when $\delta \simeq \sqrt{\nu t} \approx b$, a condition soon reached in the present case (figure 7).

(*c*) *Dynamic buckling with a linear stress profile*

Owing to skin friction, in glycerol, when the front reaches the clamped end its shape is approximately a straight line. Indeed, $\epsilon = \mathrm{erf}(x/2\sqrt{DT}) \sim x/2\sqrt{DT}$ for $x \ll \sqrt{DT}$. Thus, as an approximate model, we consider the rebound of a linear

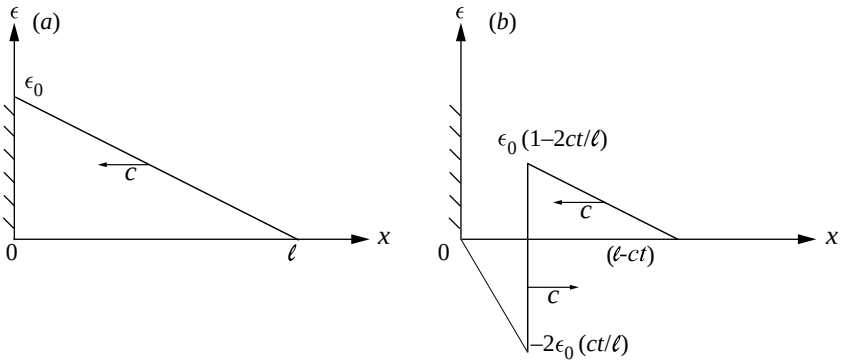

Figure 9. (*a*) Linear strain profile reaching the clamped end with velocity c. (*b*) Strain profile at time t after the rebound at the clamped end.

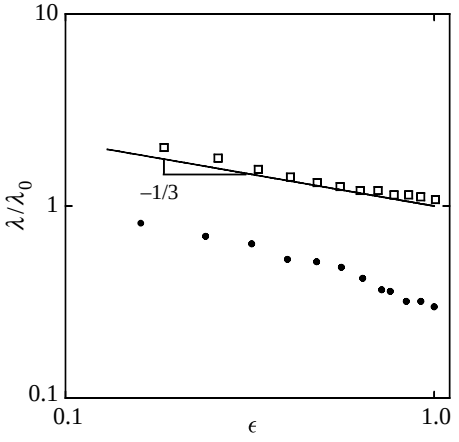

Figure 10. Buckled wavelength versus initial stretching in log–log scale with $\lambda_0 = 2(\pi^2 h^2 \ell/12)^{1/3}$. Open square, measurements in glycerol $\eta = 0.650$ Pa s; and filled circle, measurements in air. The continuous line shows the theoretical curve (equation 4.13) with no adjusted parameter.

front moving at a velocity c towards the clamped end. When the stress-free front reaches the clamped end at $t=0$, the strain profile has the form $\epsilon(x) = \epsilon_0(1 - x/\ell)$ as shown in figure 9*a*.

At time t, the front rebounds and in the section behind the rebounding front $(0 \leq x \leq \ell - ct)$, the stretching is $\epsilon(x) = -2\epsilon_0 x/\ell$. At time t, the mean compressive force behind the front is $T_\mathrm{m} = -(Ebhct/\ell)\epsilon_0$. We consider that buckling starts when the front has reached the length $\lambda/2$ where $\lambda = (|T_\mathrm{m}|/2EI)^{1/2}$ is the wavelength selected by dynamic buckling and thus we obtain

$$\lambda = 2\left\{\frac{\pi^2 h^2 \ell}{12\epsilon_0}\right\}^{1/3}. \tag{4.13}$$

The same method applied to the case of a discontinuous front results in the following expression of the buckled wavelength: $\lambda = \pi h\sqrt{2/3\epsilon_0}$ as it is known and discussed in §3*b*, considering $\epsilon_0 \ll 1$. A satisfactory comparison with the experimental measurements of the buckled wavelength is shown in figure 10. This approach

shows that taking into account the spreading of the front is sufficient to explain the greater observed wavelengths. Therefore, the increase of the buckled wavelength is not due to viscous effects involved during the dynamic buckling itself.

5. Conclusion

The main phenomena involved in the recoil of an initially stretched rubber band are the propagation of an axial-stress front, its rebound and the development of a buckling instability. A simple description of longitudinal and transverse elastic waves provides a good insight on the dynamics. The main point is that, at early stage of the recoil, the wavelength is correctly predicted in this framework at least for moderate initial elongation (i.e. $\epsilon_0 < 1$).

At higher initial strain, the wavelength becomes of the order of the band thickness and the long wave description is no longer appropriate. Three-dimensional deformations lead to even smaller wavelength. Once the band is wrinkled, the axial stress relaxes by a simple geometrical effect leading to a coarsening of the initial undulations.

When the rubber band is immersed in a fluid, the major effect is the spreading of the initial front owing to boundary layer friction. The smoother stress profile leads to longer wavelength, and a simple model based on a linear compressive strain profile gives a good estimate of the most amplified wavelength. Added mass effects slow down the instability but do not modify mode selection appreciably. The impact of both fluid viscosity and density on the instability development are quantified with appropriate dimensionless numbers.

It was not necessary to account for a possible nonlinear elastic response of the material.

This work was supported by the Agence Nationale de la Recherche through the grant ANR-05-BLAN-0222-01. R.V. was supported by the Délégation Générale à l'Armement.

Appendix A. Dispersion relation for the buckling of a rod interacting with a surrounding fluid.

We derive the dispersion relation (equation (4.1)) for waves propagating along the rubber band in a viscous fluid, in two dimensions. In the reference state, the elastic rod is of infinite extent in the x-direction and its thickness is h. The two fluid domains, denoted by the index 1 for the upper domain ($y > 0$ in the reference configuration) and 2 for the lower domain separated by the rubber band. The model is based on the linearized Navier–Stokes equation for the two fluid domains.

$$\rho \frac{\partial U_{1,2}}{\partial t} = -\frac{\partial P_{1,2}}{\partial x} + \eta \left(\frac{\partial^2 U_{1,2}}{\partial x^2} + \frac{\partial^2 U_{1,2}}{\partial y^2} \right), \tag{A 1}$$

$$\rho \frac{\partial V_{1,2}}{\partial t} = -\frac{\partial P_{1,2}}{\partial y} + \eta \left(\frac{\partial^2 V_{1,2}}{\partial x^2} + \frac{\partial^2 V_{1,2}}{\partial y^2} \right). \tag{A 2}$$

The fluid is incompressible. Thus, $\nabla^2 P_{1,2}=0$ and we look for P_1 and P_2 of the form

$$P_1 = p_1^{(0)} + p_1 \exp(-ky)\exp(\sigma t - \mathrm{i}kx), \tag{A 3}$$

$$P_2 = p_2^{(0)} + p_1 \exp(ky)\exp(\sigma t - \mathrm{i}kx), \tag{A 4}$$

where we have used the condition that pressure must remain finite at infinity. We look for $V_{1,2}$ of the form

$$V_{1,2} = v_{1,2}(y)\exp(\sigma t - \mathrm{i}kx). \tag{A 5}$$

Using these forms for $P_{1,2}$ and $V_{1,2}$ in equations (A 1) and (A 2), we have

$$q^2 v_1 - \frac{\partial^2 v_1}{\partial y^2} = -\frac{k}{\eta} p_1 \exp(-ky), \tag{A 6}$$

$$q^2 v_2 - \frac{\partial^2 v_2}{\partial y^2} = \frac{k}{\eta} p_2 \exp(-ky), \tag{A 7}$$

where

$$q^2 = \frac{\rho\sigma}{\eta} + k^2. \tag{A 8}$$

Thus, for V_1 and V_2, we have (using the condition that V must remain finite)

$$V_1 = \{A_1 \exp(-qy) + B_1 \exp(-ky)\}\exp(\sigma t - \mathrm{i}kx), \tag{A 9}$$

$$V_2 = \{A_2 \exp(qy) + B_2 \exp(ky)\}\exp(\sigma t - \mathrm{i}kx), \tag{A 10}$$

with

$$p_1 = \frac{\eta}{k}(q^2 - k^2)B_1 \text{ and } p_2 = \frac{\eta}{k}(q^2 - k^2)B_2. \tag{A 11}$$

We use the continuity equations

$$\frac{\partial U_{1,2}}{\partial x} + \frac{\partial V_{1,2}}{\partial y} = 0, \tag{A 12}$$

to obtain $U_{1,2}$

$$U_{1,2} = -\frac{1}{\mathrm{i}k}\frac{\partial V_{1,2}}{\partial y}. \tag{A 13}$$

There are four boundary conditions at the interface between the fluid and rod.

- Assuming that the cross-sections of the rod are moving along the y-direction without being stretched or compressed, the transverse displacement is homogenous in a section yielding the kinetic conditions at both interfaces ($y=\pm h/2$) in the transverse direction

$$V_1|_{y=h/2} = V_2|_{y=-h/2} = \frac{\partial \xi}{\partial t}. \tag{A 14}$$

- With a fluid initially at rest and in the slender slope limit, the difference of horizontal velocity across a section is

$$U_1|_{y=h/2} - U_2|_{y=-h/2} = -h\frac{\partial^2 \xi}{\partial t \partial x}. \tag{A 15}$$

Then, neglecting the thickness of the rod h versus the wavelength $\lambda = 2\pi/k$, the equation (A 15) leads to the kinetic condition in the axial direction

$$U_1|_{y=h/2} = U_2|_{y=-h/2}. \tag{A 16}$$

- Moreover, we are looking for modes that are anti-symmetrical across the medium line, i.e. such that

$$\Gamma_{xy,1} = \Gamma_{xy,2}, \tag{A 17}$$

where $\Gamma_{xy,1,2}$ is the xy term of the viscous stress tensor in the fluid. This condition also states that the shear stress at the rod surface is anti-symmetrical.

- For the transverse motion of the rod, we use an Euler–Bernoulli model

$$\rho_0 S\frac{\partial^2\xi}{\partial t^2} + EI\frac{\partial^4\xi}{\partial x^4} + T\frac{\partial^2\xi}{\partial x^2} + b\Delta\left[-P_{1,2} + \boldsymbol{n}_2\cdot\left(\hat{\boldsymbol{\Gamma}}_{1,2}\,\boldsymbol{n}_{1,2}\right)\right] = 0, \tag{A 18}$$

where the last term of the left-hand side represents the fluid-stress difference between both sides of the rod. $\hat{\boldsymbol{\Gamma}}_{1,2}$ is the viscous stress tensor in the fluid and $\boldsymbol{n}_{1,2}$ is the vector normal to the interface. $\hat{\boldsymbol{\Gamma}}_{1,2}$ in the fluid takes the form

$$\hat{\boldsymbol{\Gamma}}_{1,2} = \begin{pmatrix} \eta\dfrac{\partial U_{1,2}}{\partial x} & \dfrac{\eta}{2}\left(\dfrac{\partial U_{1,2}}{\partial y} + \dfrac{\partial V_{1,2}}{\partial x}\right) \\ \dfrac{\eta}{2}\left(\dfrac{\partial U_{1,2}}{\partial y} + \dfrac{\partial V_{1,2}}{\partial x}\right) & \eta\dfrac{\partial V_{1,2}}{\partial y} \end{pmatrix}. \tag{A 19}$$

At leading order, we have $\boldsymbol{n}_1 = -\boldsymbol{n}_2 = (-\partial\xi/\partial x, 1)$ and thus,

$$\Delta\left[\boldsymbol{n}_2\cdot(\hat{\boldsymbol{\Gamma}}_{1,2}\boldsymbol{n}_{1,2})\right] = 2\eta\left(\frac{\partial V_2}{\partial y}|_{y=h/2} - \frac{\partial V_1}{\partial y}|_{y=-h/2}\right) \tag{A 20}$$

Using these four conditions in equations (A 6), (A 7) and (A 14), we obtain a dispersion equation for the dynamic buckling of the rod in the fluid

$$A_1 - A_2 = (B_2 - B_1)\exp\left[\frac{(q-k)h}{2}\right]. \tag{A 21}$$

Using the form of $U_{1,2}$ (equation (A 13)) and equation (A 16), we obtain

$$A_1 + A_2 = -\frac{k}{q}(B_2 + B_1)\exp\left[\frac{(q-k)h}{2}\right]. \tag{A 22}$$

And finally, from the relation between tangential stress (equation (A 17)) and using the forms of V (equations (A 9) and (A 10)) and U (equation (A 13)), we get

$$A_1 - A_2 = \frac{2k^2}{q^2 + k^2}(B_2 - B_1)\exp\left[\frac{(q-k)h}{2}\right]. \tag{A 23}$$

Combining equations (A 21) and (A 23) and using equation (A 11), we have

$$A_1 = A_2, \tag{A 24}$$

$$B_1 = B_2, \tag{A 25}$$

$$p_1 = -p_2. \tag{A 26}$$

Using equation (A 22), we find

$$A_1 = -\frac{k}{q} B_1 \exp\left[\frac{(q-k)h}{2}\right]. \tag{A 27}$$

We write $\Delta(-P_{1,2} + \boldsymbol{n}_2 \cdot \hat{\boldsymbol{\Gamma}}_{1,2} \boldsymbol{n}_{1,2}))$ in terms of B_1,

$$\begin{aligned} &\Delta(-P_{1,2} + \boldsymbol{n}_2.(\hat{\boldsymbol{\Gamma}}_{1,2} \boldsymbol{n}_{1,2})) \\ &\quad = \left\{(p_1 - p_2)\mathrm{e}^{-kh/2} + \eta q(A_1 + A_2)\mathrm{e}^{-qh/2} + \eta k(B_1 + B_2)\mathrm{e}^{-kh/2}\right\}\mathrm{e}^{\sigma t - \mathrm{i}kx} \\ &\quad = \left\{2\frac{\eta(q^2 - k^2)}{k} B_1 \mathrm{e}^{-kh/2}\right\}\mathrm{e}^{\sigma t - \mathrm{i}kx}. \end{aligned} \tag{A 28}$$

The expression of ξ is obtained from the transversal boundary condition (equation A 14)

$$\xi = \frac{1}{\sigma}\{A_1 \mathrm{e}^{-qh/2} + B_1 \mathrm{e}^{-kh/2}\}\mathrm{e}^{\sigma t - \mathrm{i}kx}. \tag{A 29}$$

Introducing this expression in (A 18) and using relations (A 21) and (A 28), we obtain the dispersion equation

$$\left(\rho_0 S + 2\frac{\rho b}{k}\right)\sigma^2 + 2b\eta(k + q)\sigma + EIk^4 - Tk^2 = 0. \tag{A 30}$$

In dimensionless form, this relation reads

$$\{k_* + 4M\}\sigma_*^2 + 4\chi k_* \left\{k_* + \left(\frac{M}{\chi}\sigma_* + k_*^2\right)^{1/2}\right\}\sigma_* + 4k_*^3\left(k_*^2 - 1\right) = 0, \tag{A 31}$$

with $k_* = k/k_\mathrm{c}$ and $\sigma_* = \sigma/\sigma_\mathrm{m}$. The two dimensionless coefficients are

$$\chi = \left(\frac{\eta^2 b}{\rho_0 Th}\right)^{1/2} \text{ and } M = \frac{\rho\lambda_c}{4\pi\rho_0 h}. \tag{A 32}$$

References

Bouasse, H. & Carrière, Z. 1903 Sur les courbes de traction du caoutchouc vulcanisé. *Annales de la faculté des sciences de Toulouse, 2e série* **5**, 257–283.

Euler, L. 1744 Addidentum I de curvis elasticis, methodus inveniendi lineas curvas maximi minimivi proprietate gaudentes. In *Opera Omnia I*, pp. 231–297. Lausanne.

Gladden, J. R., Handzy, N. Z., Belmonte, A. & Villermaux, E. 2005 Dynamic buckling and fragmentation in brittle rods. *Phys. Rev. Lett.* **94**, 035503. (doi:10.1103/PhysRevLett.94.035503)

Graff, K. G. 1975 *Wave motion in elastic solids*. New York, NY: Dover Publications.
Kolsky, H. 1949 An investigation of the mechanical properties of materials at very high rates of loading. *Proc. Phys. Soc. B* **62**, 676–700. (doi:10.1088/0370-1301/62/11/302)
Lamb, H. 1932 *Hydrodynamics*. Cambridge, UK: Cambridge University Press.
Lepik, U. 2001 Dynamic buckling of elastic-plastic beams including effects of axial stress waves. *Int. J. Impact Eng.* **25**, 537–552. (doi:10.1016/S0734-743X(00)00070-1)
Lindberg, H. E. 1965 Impact buckling of a bar. *J. Appl. Mech.* **32**, 315–322.
Love, A. E. H. 1944 *A treatise on the mathematical theory of elasticity*, 4th edn. New York, NY: Dover Publications.
Mason, P. 1963 Finite elastic wave propagation in rubber. *Proc. R. Soc. A* **272**, 315–330.
Mullins, L. 1947 Effect of stretching on the properties of rubber. *J. Rubber Res.* **16**, 275–289.
Saint-Venant, M. & Flamant, A. 1883 Résistance vive ou dynamique des solides. Représenttaion graphique des lois du choc longitudinal, subi à une des extrémités par une tige ou barre prismatique assujettie à l'extrémité opposée. *C.R. Acad. Sci.* **97**, 127–133.
Stokes, G. G. 1850 On the effect of the internal friction of fluids on the motion of pendulums. *Trans. Camb. Phil. Soc.* **IX**, 8 sec 52.
Vaughn, D. G. & Hutchinson, J. W. 2006 Bucklewaves. *Eur. J. Mech. A/Solids* **25**, 1–12. (doi:10.1016/j.euromechsol.2005.09.003)